Pol. J. Environ. Stud. Vol. XX, No. X (XXXX), 1-9
DOI: *10.15244/pjoes/206956* ONLINE PUBLICATION DATE: 2025-09-15

Original Research

Electrocatalytic Water Splitting Potential of *Cymbopogon citratus*-Mediated Biosynthesized Strontium Oxide Nanoparticles

Amna Murad[1], Muhammad Sagir[2], Shazma Massey[3], Zahida Nasreen[4], Assad Amanullah[5], Tauqeer Ahmad[6], Shabbir Hussain[1]*, Ayesha Kiran[1], Khalid Mashay Al-Anazi[7], Mohammad Abul Farah[7], Asif Ali Tahir[8]

[1]Institute of Chemistry, Khwaja Fareed University of Engineering and Information Technology, Rahim Yar Khan 64200, Pakistan
[2]Institute of Chemical and Environmental Engineering, Khwaja Fareed University of Engineering and Information Technology, Rahim Yar Khan 64200, Pakistan
[3]Department of Chemistry, Forman Christian College (A Chartered University) Lahore 54600, Pakistan
[4]Department of Zoology, University of Mianwali, 42200, Pakistan
[5]Department of Chemistry, University of Lahore Sargodha Campus, Pakistan
[6]Institute of Chemistry, University of Sargodha, 40100, Pakistan
[7]Department of Zoology, College of Science, King Saud University, `Riyadh 11451, Saudi Arabia
[8]Director of Research Engineering (Penryn Campus), Environment and Sustainability Institute, University of Exeter, Penryn Campus, Penryn, TR10 9FE, UK

Received: 11 September 2024
Accepted: 10 June 2025

Abstract

Strontium-based nanoparticles (NPs) find applications in energy storage, electronics, optoelectronic devices, lightning, FETs, LEDs, television screens, display units, fabrication of sensors, wastewater treatment, vehicles of space and navigation, remote weather stations, and in the field of medicine (antibacterial agents, tissue engineering, orthopedics, bone regeneration, bone health, and in the treatment of osteoporosis, etc.). Recently, plant-mediated green synthesis of NPs has gained significant attention due to its eco-friendly, sustainable, and cost-effective approach. The green production of strontium oxide (SrO) NPs is rarely reported in earlier literature, which is the focus of the current study. We synthesized SrO_{aq} and SrO_{et} NPs by utilizing the aqueous and ethanolic extracts of *Cymbopogon citratus* (lemon grass). The synthesized NPs were analyzed by FTIR, X-ray diffraction (XRD), and UV-visible spectroscopies. FTIR analysis showed the presence of organic moieties and characteristic Sr-O bands. UV-visible spectroscopy displayed an absorption peak at 298 and 298.9 nm in SrO_{aq} and SrO_{et}, respectively. SrO_{et} exhibited a smaller band gap (4.25 eV) than SrO_{aq} (4.47 eV). The synthesized NPs

*e-mail: shabchem786@gamil.com;
shabbir.hussain@kfueit.edu.pk
Tel.: +92-321-4140130

possessed well-defined crystalline structures and exhibited good electrocatalytic performance for water splitting. SrO_{et} was found to be a more effectual electrocatalyst for oxygen evolution reaction (OER) and hydrogen evolution reaction (HER) due to its higher electrochemically active surface area (EASA) and smaller charge transfer resistance (R_{ct} = 60Ω) than those of SrO_{aq}. The investigated NPs displayed promising redox behavior, charge storage capacity, and catalytic efficiency, highlighting their potential usage in energy storage and electrocatalytic water splitting.

Keywords: *Cymbopogon citratus*, biosynthesis, SrO, electrocatalyst, water-splitting

Introduction

Nanotechnology has played a vital role in developing industry and technology, especially in transportation, food safety, homeland security, electronic technology, and medical and agricultural fields [1]. Nanoparticles (NPs) possess fantastic electrochemical [2], photocatalytic [3], sensing [4], anti-termite [5], therapeutic [6], and biological [7] properties, especially in their role in fuel cells [8] and supercapacitors [9], which is well recognized. They also play an important role in environmental sustainability and are useful in eliminating toxic dyes [10] and heavy metals [11] from wastewater.

Among metal oxides, strontium oxide (SrO) NPs demonstrate exceptional electrochemical performance, photocatalytic activity, good optical properties, and excellent thermal stability. These materials are promising candidates for improving battery efficiency and energy storage applications, particularly in lithium-ion batteries. They find numerous applications in electronics, lighting, wastewater treatment, etc. SrO NPs also contribute to healthier and cleaner environments because they can adsorb and immobilize contaminants and are helpful in the elimination of heavy metals and other pollutants from water and soil. They have been utilized in optoelectronic devices, FETs, LEDs, and the fabrication of sensors [12]. Strontium is used in flares, fireworks, and zinc metal refining. It is also used in plastic and paints as strontium aluminate [13]. Strontium can be used in small amounts in vacuum tubes to remove the last traces of air. It also finds applications in television screens, display units, remote weather stations, and vehicles of space and navigation [14]. In the field of biomedicine, strontium-based NPs are employed in orthopedics, bone regeneration, tissue engineering, and treatment of osteoporosis for enhancing osteoblast activity and improving bone health [13]. They have also been found effective against various strains of bacteria [12]. Strontium can control the insulin's release and is helpful in the regulation of diabetes pathophysiology [14].

NPs can be synthesized by different procedures, including gas condensation, vacuum deposition, vapor deposition and condensation, precipitation method, ball milling, direct current, electrodeposition, and the sol-gel method [15, 16]. However, green synthesis of NPs is a topic of great interest today [17] because this route is eco-friendly and cost-effective [18] and commonly involves plant materials as reducing and stabilizing agents in the synthetic route [19].

Plant-mediated synthesis of strontium-based NPs has rarely been reported in earlier literature. Moreover, the biosynthesis of SrO NPs utilizing the leaf extract of *Cymbopogon citratus* (lemongrass) has never been reported earlier, which is the focus of the current study. The structural studies of the NPs were performed using FTIR, XRD, and UV-visible characterizations. Finally, the NPs were investigated for their electrochemical potential by cyclic voltammetry (CV) and electrocatalytic water splitting potential (HER and OER). Their charge transfer resistance (R_{ct}) and electrochemically active surface area (ECSA) were also determined.

Materials and Methods

Analytical-grade chemicals, including strontium nitrate, sodium hydroxide (NaOH), and ethanol, were used for the synthesis. Pyrex-origin glassware was used, which was carefully washed with distilled water and dried in an oven before use.

Leaves of *C. citratus* were collected from Chack 49p (near Aab Hayat Canal) of Rahim Yar Khan, Pakistan, in April 2023. The Department of Life Sciences, Khwaja Fareed University of Engineering and Information Technology, Rahim Yar Khan, Pakistan, identified the plant species. The leaves were repeatedly washed with distilled water to remove all the dust and impurities. The samples were dried to eliminate any residual moisture and finally crushed into powder.

The crystallite sizes and crystallinity phase nature of the biosynthesized SrO_{aq} and SrO_{et} NPs were determined by the X'Pert Powder X-Ray Diffractometer. A Brukker-type IFS 66V FTIR spectrometer was used for the FT-IR spectroscopy of NPs. UV-visible spectra were recorded using a BIOBASE BK-D560.

Preparation of Aqueous/Ethanolic Extracts of *Cymbopogon citratus*

10 g of crushed leaves of *C. citratus* were added to 200 mL of distilled water in a round-bottom flask, and the mixture was stirred at 55°C for 2 h until its color turned light yellow. It was subsequently cooled to room

Table 1. Synthetic conditions and properties of previously reported SrO NPs in various plant extracts.

Sr. No.	Leaf extract	Strontium salt precursor	Forms and sizes of NPs	Applications tested	Reference
1	*Elodea canadensis*	Strontium nitrate	SrO = 209-217 nm, Face-centered cubic crystalline	Biomedical applications	[20]
2	*Ocimum sanctum*	Strontium nitrate	SrO = 250-350 nm, crystalline structures	Antibacterial activity	[21]
3	*Albizia julibrissin*	Strontium nitrate hexahydrate in the presence of NaOH	SrO = 20-30 nm, spherical-shaped	Treatment of industrial wastewater	[22]
4	*Vitis vinifera*	Strontium nitrate in the presence of NaOH	SrO = 20-50 nm, small-spherical shaped	Production approach in industrial areas	[23]

temperature and finally filtered through Whatman filter paper No. 1, leaving the filtrate as an aqueous extract behind.

For the formation of ethanolic extract, 12 g of powder of *C. citratus* leaves was added to 250 mL of ethanol in a round-bottom flask, and the mixture was vigorously stirred for 2 h at room temperature. Finally, it was filtered through Whatman filter paper No. 1, leaving the ethanolic extract as filtrate.

Biosynthesis of SrO_{aq} and SrO_{et} NPs

0.4 g of strontium nitrate was mixed into 50 mL of distilled water to prepare a clear solution. Then, 8 mL aqueous extract of *C. citratus* was added, which was followed by continuous stirring at 55°C. After 15 min, a few drops of dilute NaOH solution were added until the pH of the solution turned from acidic to basic. After a few minutes, the reaction mixture changed from pale yellow to dark brown, and then it was further stirred for 1.5 h. Finally, the solution was kept at room temperature for about 12 h until the NPs were settled down as precipitates, which were separated and collected by centrifugation (7,000 rpm, 7 min). The collected precipitates were subjected to washing, firstly with distilled water and then with ethanol. After drying in an oven, the NPs were finally calcined at 300°C for 5 h to leave behind the solid SrO_{aq}.

For the preparation of SrO_{et} NPs, a solution of 0.4 g strontium nitrate in 10 mL distilled water was stirred with an 8 mL ethanolic extract of *C. citratus* leaves at 55°C for 1 h, followed by the addition of a few drops of dilute NaOH until the solution became alkaline. The obtained mixture was left overnight and centrifuged to separate the precipitated NPs (7,000 rpm, 7 min). The precipitates were washed with ethanol thrice and finally calcined at 300°C for 5 h to leave behind the solid SrO_{et}.

Electrochemical Studies

Corrtest CS2350 (electrochemical workstation) was used for the electrochemical measurements. After electrodeposition, the biosynthesized SrO_{aq} and SrO_{et} NPs were utilized directly as the working electrodes on nickel foam (NF). The Ag/AgCl (1 M KCl) and Pt wire were used as reference and counter electrodes, respectively. All potentials were calibrated to a reversible hydrogen electrode (RHE). Polarization curves were drawn by performing linear sweep voltammetry (LSV) and cyclic voltammetry (CV) at a scan rate of 10 mV S^{-1}. Electrochemical impedance spectra (EIS) were recorded at 1.53 (Potential vs RHE) and a frequency range of 0.1-100000 Hz in 1 M KOH electrolyte. The double layer capacitance (Cdl) of the tested electrodes in 1 M potassium hydroxide (KOH) was used to compute the electrochemically active surface area (ECSA) by applying the following equation: ECSA = Cdl/Cs.

Results and Discussion

In the current study, we have synthesized SrO_{aq} and SrO_{et} NPs by utilizing the aqueous and ethanolic extracts of *C. citratus*. The NPs were analyzed by XRD, FTIR, and UV-visible spectroscopy and were also investigated for their electrocatalytic water-splitting potential.

Green synthesis has attracted the focus of material energy scientists due to its eco-friendly and sustainable pathways. It often utilizes readily available, natural, and sustainable resources, thus reducing the need for expensive reagents and specialized equipment. Earlier studies had reported the biosynthesis of SrO NPs only in *Elodea canadensis* [20], *Ocimum sanctum* [21], *Albizia julibrissin* [22], and *Vitis vinifera* [23] (Table 1), but there are still no reports on the production of *C. citratus*-mediated SrO. We have chosen *C. citratus* leaves to prepare strontium oxide NPs because this plant is an important source of numerous phytochemical and antioxidant constituents (Table 2) [24]. The aqueous and ethanolic extracts of *C. citratus* contained 4.07 and 47.09 mg/100 g, respectively, of total phenolic content (TPC) and 2.43 and 65.09 mg/100 g, respectively, of total flavonoid content (TFC). The ethanolic extract of *C. citratus* is a better source of phenolics (e.g., caffeic acid, gallic acid, and sinapic acid) and flavonoids (e.g., myricetin) compared to its aqueous counterpart

Table 2. Important phytochemical constituents in aqueous/ethanolic extracts of *C. citratus leaves* [24].

C. citratus aqueous extract	*C. citratus* ethanolic extract
3-hydroxy-3-methylbutanoic acid, Acetic acid, Cis-linaloloxide, Neric acid, 2-Methyl resorcinol, Trans-7-oxabicyclo[4.3.0]nonane, Glycerol-1-palmitate, 2 methoxy 4-vinylphenol, 3-Tetradecanol, Phytyl heptadecanote, Longipinane, 2-methyl-2-pentenal, 3,5,5-trimethyl cyclohexene, Epoxy-linalooloxide, Hexanamide, Butanal, 6-methylheptane-1,6 diol, Neral, Benzeneacetic acid, Enanthamide, Triallylvinylsilane, Mequinol, Decamethyl cyclopentasiloxane, Dodecamethyl cyclohexasiloxane, Geranic acid, 3-Hexen-1ol, Isophtol,acetate, Dimethylmorpholinophosphoramidate, Alpha-ferpinyl acetate, Homovanillyl alcohol, Methyl stearate, 3-Octyme, 3-Aminopiperidin-2-one, Benzoic acid,hydrazide, 2-pyrrolidinone, 2-Hexyldodecyl acetate, Methenamine, 2-Oxaadamantane, Pentanamide, 5-hexyn-1-ol, 2-ethyl 2-butenal, *n*-Hexadecanoic acid, 1-Ethoxy 2-heptanone, 2-Buten-1-ol, 3-methyl-acetate	Lupeol, *n*-Hexadecanoic acid, *B*-sitosterol, Phytol, Benzofuran, 2,3-dihydroxyl, A-Friedoursan-3-one, Geranic acid, Stigmasterol, Glycerol 1-palmitate, 5-Nonen-2-one, Neophytadiene, 1-butanol,3-methoxy-acetate, Linoelaidic acid, Linoelaidic acid, Campesterol, Cholesterol, 5-nitro 4-nonene, 2,2,2-trifluoro acetamide, Geranyl capryl-, 6-Hydroxy-4,4,7a-trimethyl, 4-ethenyl-2,6-phenol, 2,3-Dimethyl-3-heptene, Hexadecanoic acid, Vitamin E, Heptadecanoic acid, Vitamin E, Hexadeca-tetraen-1-ol, Hexadeca-2 tetraen-1-ol, 2,15-Hexadecaedione,

(extract), which contains only caffeic acid (phenolic) [24]. These phytochemicals and antioxidants enable *C. citratus* leaves to act as good reducing and stabilizing agents for generating SrO NPs from strontium nitrate. The leaf extracts of *C. citratus* were prepared using water and ethanol solvents, which are easily available and have no toxic side effects.

Structural Studies

The XRD graphs of SrO_{aq} and SrO_{et} NPs have shown almost the same XRD patterns (Fig. 1). The diffraction peaks in SrO_{aq} were displayed at 2θ values of 31.86, 36.6, 50.36, 64.11, and 74.25°, which correspond to the Miller indices of (111), (200), (220), (311), and (400), respectively (Fig. 1a)). In SrO_{et} NPs, the most intense and characteristic diffraction peaks appeared at 31.5, 36.8, 50.2, 64.8, and 74.39°, which can be assigned to the (111), (200), (220), (311), and (400) crystal planes, respectively (Fig. 1) [25]. Both SrO_{aq} and SrO_{et} NMs displayed cubic structures [26] with JCPD card number 74-1227 [27]. The crystalline sizes were calculated using the Debye–Scherrer Equation [28] and were found to be 31.62 and 28.43 nm for SrO_{aq} and SrO_{et} NPs, respectively. The smaller crystalline size of SrO_{et} indicates its greater surface area than that of SrO_{aq}. The larger surface area results in an enhanced surface-to-volume ratio of NPs and improves their reactivities [29]. The obtained results are thus in complete agreement with the higher electrocatalytic water splitting (HER and OER) performance of SrO_{et} than of SrO_{et}, which will be discussed in the coming sections.

Fourier Transform Infrared Spectroscopy (FTIR)

The FT-IR spectra of the synthesized NPs were recorded in the wave number range of 400-4000 cm^{-1} and are shown in Fig. 2. The FTIR spectroscopy displayed the existence of Sr-O vibrations, which appeared at 546 and 531 cm^{-1} in SrO_{aq} and SrO_{et}, respectively [30]. The obtained spectra (Fig. 2) have also shown the presence of aliphatic (C-H), hydroxyl (-OH), and carbonyl (C=O) compounds; these organic moieties are attributed to the coating of plant extracts upon the surfaces of biosynthesized NPs.

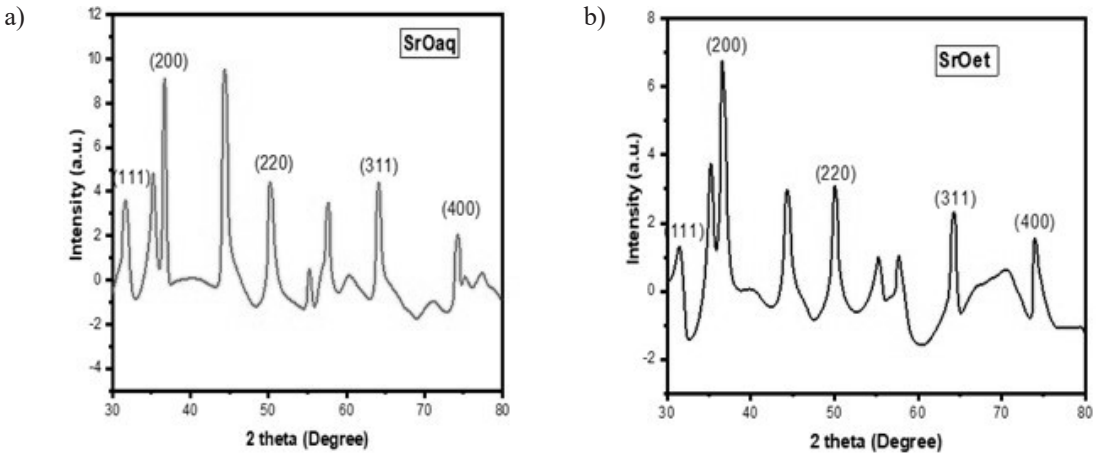

Fig. 1. XRD spectra of a) SrO_{aq} and b) SrO_{et} nanoparticles synthesized using aqueous and ethanolic extracts, respectively, of *C. citratus* leaves.

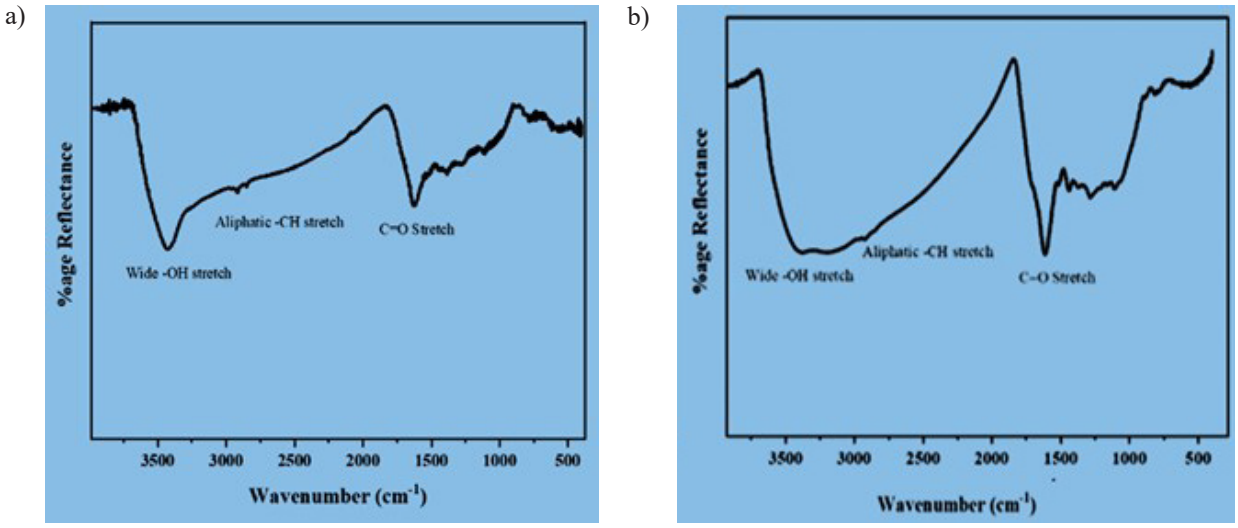

Fig. 2. FT-IR spectra of a) SrO_{aq} and b) SrO_{et}.

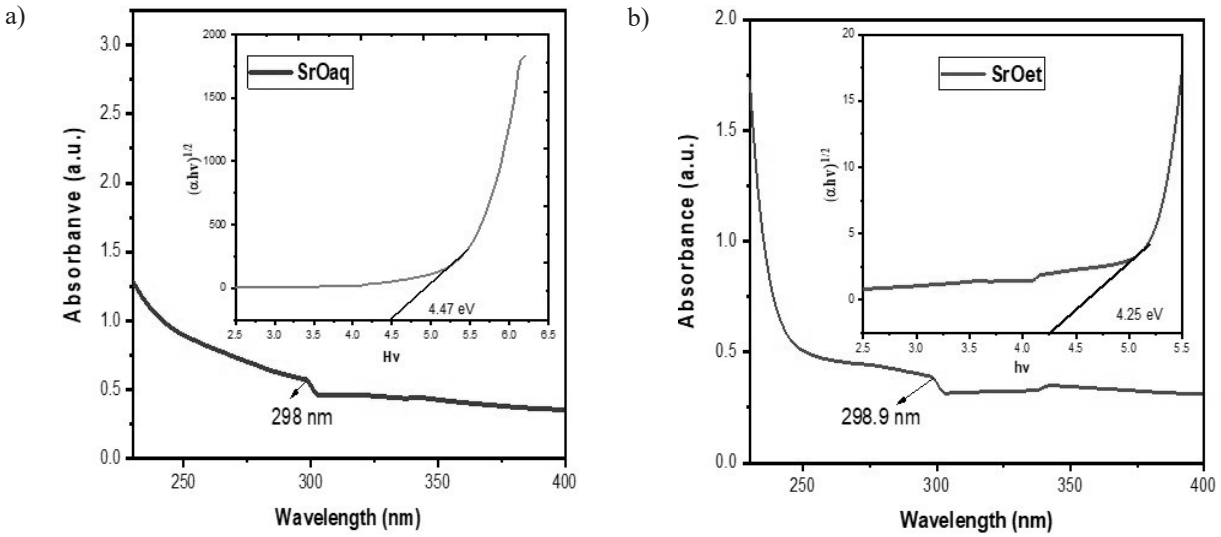

Fig. 3. UV-visible spectra and band gaps of a) SrO_{aq} and b) SrO_{et} NPs.

UV-Visible Analysis

The optical studies of SrO_{aq} and SrO_{et} nanostructures were performed at room temperature in the range of 200 to 400 nm. The UV-visible spectra are shown in Fig. 3. A strong absorption was observed at 298.0 and 298.9 nm (representing the band edge transition) in SrO_{aq} and SrO_{et}, respectively, revealing the sample's photoelectrical characteristics. The band gaps of the investigated nanoparticles were calculated using Tauc's Equation (Eq. (1)).

$$(\alpha hv)^n = A(hv - E_g) \tag{1}$$

Where v is the energy of the photon, a is the coefficient of absorption, h is Planck's constant, n = 1/2 for an indirect transition and n = 2 for a direct transition, E_g is the energy of the band gap, and A represents the proportionality constant [31]. It was found (Fig. 3) that SrO_{et} has a smaller band gap (4.25 eV) than that of SrO_{aq} (4.47 eV). The smaller band gap of a nanomaterial contributes to its electrocatalytic water-splitting efficiency [32]. The obtained results thus clarify the higher catalytic potential of SrO_{et} than that of SrO_{aq}, which will be discussed in the coming sections.

Oxygen Evolution Reaction (OER)

The oxygen evolution reaction (OER) serves as a rate-determining step in alkaline water electrolysis. The OER of the tested SrO_{aq} and SrO_{et} electrodes on the Ni foam was performed in a 1 M potassium hydroxide solution at a scan rate of 10 mV/s; the obtained LSV OER data are graphically plotted in Fig. 4.

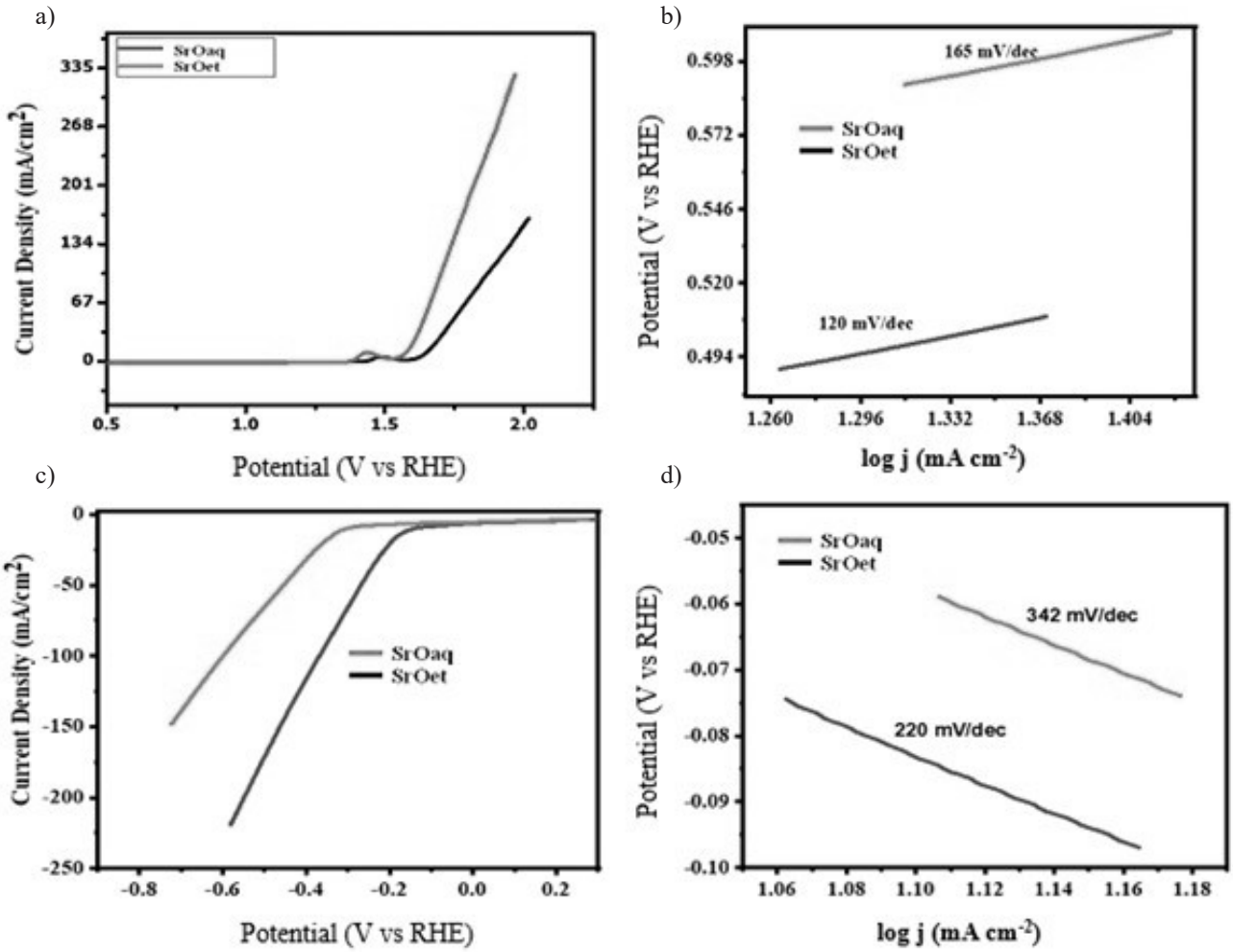

Fig. 4. LSV OER curves of a) SrO_{aq} and SrO_{et} and b) their corresponding Tafel slopes; LSV HER curves of c) SrO_{aq} and SrO_{et} and d) their corresponding Tafel slopes.

It was found that an onset potential of 1.51 and 1.59 (Potential vs RHE) was required by SrO_{et} and SrO_{aq} electrocatalysts, respectively, to initiate the OER process (Fig. 4). The excellent catalytic effectiveness of the SrO_{et} electrocatalyst was reflected in its significantly higher value of current density (340 $mAcm^{-2}$) than that of SrO_{aq} (135 $mAcm^{-2}$) [33]. However, it is worth mentioning that both SrO_{aq} and SrO_{et} nanostructures demonstrated significantly better OER performance and enhanced ion conductivity. The SrO_{et} electrode also exhibited a lower value of Tafel slope (120 mV/dec) than that (165 mV/dec) of SrO_{aq} (Fig. 4), indicating the faster OER rate in the former. It is important to mention that the smaller Tafel slope value demonstrates a faster electrocatalytic reaction and an increased OER activity [33]. The results thus agree that SrO_{et} is one of the most effective and non-precious catalysts for oxidizing alkaline water.

Hydrogen Evolution Reaction (HER)

HER serves as the rate-determining step in water electrolysis. Fig. 4c) shows the HER curves of the biosynthesized nanomaterials. The electrocatalytic efficacy of SrO_{aq} and SrO_{et} on the Ni foam substrate toward HER in an alkaline medium was significantly higher than that of highly conductive and porous Ni foam. To initiate the HER process, the onset potential of -0.4 and -0.1 (Potential vs RHE) was used by SrO_{aq} and SrO_{et} electrocatalysts, respectively (Fig. 4). SrO_{et} electrode also exhibited a lower value of Tafel slope (176 mV/dec, Fig. 5) than SrO_{aq} (210 mV/dec), indicating faster HER kinetics in the former. According to the aforementioned findings, SrO_{et} is one of the most effective and non-precious catalysts for oxidizing alkaline water. The obtained results thus clarify that SrO_{et} is a significantly better electrocatalyst due to its lower overpotential and smaller Tafel slope and offers better HER and OER performance than that of SrO_{aq}.

Cyclic Voltammetry and Electrochemically Active Surface Area (ECSA)

We performed the CV tests at various scan rates (20 to 100 mV s^{-1}) in a potential range of 1.34-1.48 V; the obtained results are displayed in Fig. 5. The presence of clear oxidation-reduction peaks (Fig. 5) indicates

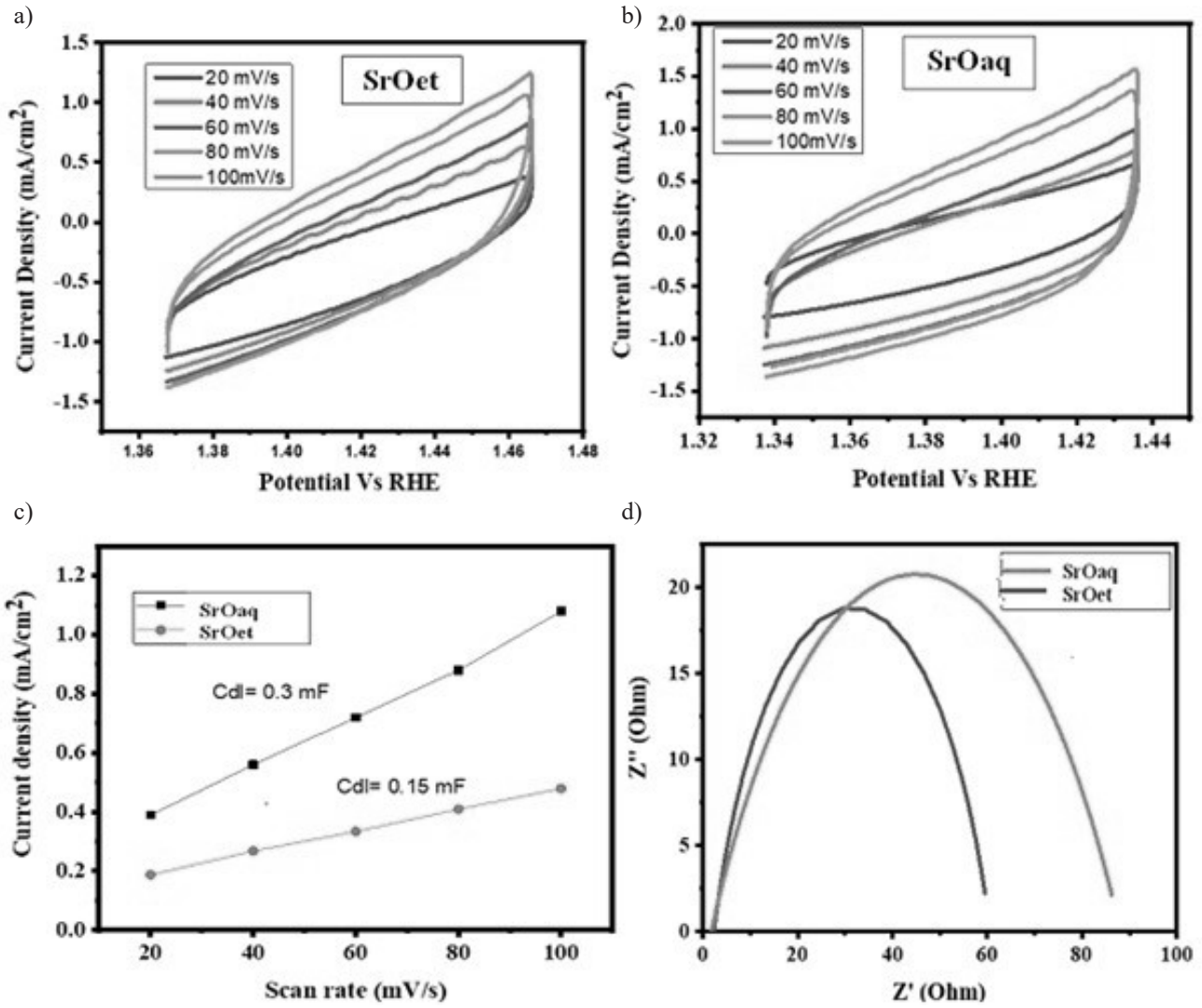

Fig. 5. a) CV Graph of SrO_{aq}; b) CV Graph of SrO_{et}; c) Cdl of SrO_{aq} and SrO_{et} at various scan rates; d) EIS of SrO_{aq} and SrO_{et}.

a reversible redox behavior and thus depicts that the charging process is reversible in the investigated SrO_{aq} and SrO_{et} nanomaterials [18, 19].

Before conducting any other electrochemical experiment, knowing about the electrochemically active surface area (ECSA) is crucial. The inherent ECSA generally indicates an electrocatalyst's active region and acts as a decisive parameter in electrocatalytic water-splitting. The differences between the current densities of the anode and the cathode were plotted against various scan rates to determine the Cdl values of the investigated NPs (Fig. 5). A greater Cdl value reflects a higher ECSA and indicates more accessible active sites. The higher value of ECSA usually supports the enhanced electrocatalytic efficiency of a catalyst [33]. The greater Cdl value of SrO_{et} (0.3 mF) than that of SrO_{aq} (0.15 mF) reflects its higher ECSA, further indicating its improved electrocatalytic characteristics in terms of OER and HER. The formula ECSA = Cdl/Cs was used to determine the ECSA. The higher ECSA value of SrO_{et} (75 cm^2) than that of SrO_{aq} (37.5 cm^2) evidently depicts the greater surface area of the former (SrO_{et}). This thus supports the higher electrocatalytic water splitting (HER and OER) potential of SrO_{et} than that of $SrO_{aq,}$ which was also discussed in the previous two sections (OER and HER).

Electrode Impedance Spectroscopy (EIS)

Electrode impedance spectroscopy (EIS) is usually performed to elucidate the OER reaction charge transfer and kinetic processes. We have performed the EIS measurements in a 100000-0.1 Hz frequency range by employing an alternating current amplitude value of 5 mV. The EIS plots are shown in Fig. 5. The charge transfer resistance (R_{ct}) value was calculated by fitting a simple Randle's circuit to the low-frequency area of the Nyquist plot. The diameter of the semicircle demonstrates the R_{ct} [33], which indicates the resistance to charge transfer of an E_{redox} reaction. EIS measurements revealed that the charge transfer resistance (R_{ct}) of SrO_{et} (60Ω) is smaller than that of SrO_{aq} (86Ω). The lower

value of R_{ct} reflects higher conductivity and speedy charge-transfer ability and minimizes the ohmic loss. The obtained results thus demonstrate a much faster electron transfer and, thus, better OER electrocatalytic efficiency of SrO_{et} than that of SrO_{aq}.

Conclusions

We successfully established a green synthetic route for producing SrO_{aq} and SrO_{et} NPs by utilizing the aqueous and ethanolic extracts of *C. citratus* leaves. The investigated NPs were analyzed by FTIR, XRD, and UV-visible spectroscopies. FTIR analysis has shown the existence of Sr-O vibrations and organic moieties in the biosynthesized nanoparticles. UV-visible spectroscopy displayed absorption peaks at 298.0 and 298.9 nm in SrO_{aq} and SrO_{et}, respectively. SrO_{aq} has shown a smaller band gap than that of SrO_{et}. Both the nanomaterials (SrO_{aq} and SrO_{et}) possessed well-defined crystalline structures and have shown good electrocatalytic water-splitting potential. However, SrO_{et} was proven to be a better OER and OER electrocatalyst due to its higher electrochemically active surface area (EASA) and smaller charge transfer resistance than SrO_{aq}. It is recommended that *C. citratus*-mediated biosynthesized strontium oxide (SrO) NPs are effective electrocatalysts and can be successfully applied for water-splitting applications.

Acknowledgments

The authors express their sincere appreciation to the Researchers Supporting Project number (RSP2025R154), King Saud University, Riyadh, Saudi Arabia.

Conflict of interest

It is hereby declared that there is no conflict of interest between the authors.

References

1. SUHAG D., THAKUR P., THAKUR A. Introduction to nanotechnology. In: Integrated Nanomaterials and their Applications, Springer Nature Singapore, **2023**.
2. KIRAN A., HUSSAIN S., AHMAD I., IMRAN M., SAQIB M., PARVEEN B., MUNAWAR K.S., MNIF W., AL HUWAYZ M., ALWADAI N. Green synthesis of NiO and NiO@ graphene oxide nanomaterials using Elettaria cardamomum leaves: Structural and electrochemical studies. Heliyon. **10** (20), **2024**.
3. ALI K.S., SHAH K.H., ASIF H.M., KHAN M.A., HUSSAIN S., TARIQ M. Synthesis, Characterization, Photocatalytic and Antimicrobial Potential of Pr_2O_3/ ZnO/gC_3N_4 Nanocomposite. International Journal of Environmental Research. **18** (4), 66, **2024**.
4. ALI K.S., ZAHOOR M.S., TARIQ M., ASIF H.M., HUSSAIN S., SHIRAZI J.H. Reduced graphene oxide with La@ Co_3O_4 and La@ CdO nanocomposite based sensors: synthesis, characterization and NO_2 sensing properties. Journal of the Iranian Chemical Society. **21** (8), 2067, **2024**.
5. JAVED M., HUSSAIN S., RIAZ M., ASGHAR A., SYED S., BARKAAT S., SULEMAN M., IDREES M., ASHRAF F., FAIZAN M. Synthesis and characterization of nanoparticles derived from chitosan-based biopolymer; their photocatalytic and anti-termite potential. Digest Journal of Nanomaterials & Biostructures. **16** (4), 1607, **2021**.
6. BIBI F., AHMAD I., HUSSAIN S., IBRAHIM M. Synergistic effect of graphene oxide and silica nanocomposites towards multifunctional biomedical applications. Ceramics International. **24**, 53319, **2024**.
7. HUSSAIN S., ASLAM A., TAJAMMAL A., OTHMAN F., MUSTAFA Z., ALSUHAIBANI A.M., REFAT M.S., SHAHID M., SAGIR M., ZAKARIA Z.A. Tagetes erecta-Mediated Biosynthesis of Mn_3O_4 Nanoparticles: Structural, Electrochemical, and Biological Investigations. ACS Omega. **9** (33), 35408, **2024**.
8. IQBAL M., MUNEER M., RAZA R., SALEEM M., HUSSAIN S., REHMAN Z.U., ABBAS F., ALI S., JAVED M.A., HUSSAIN M. Recycling of lead from lead acid battery to form composite material as an anode for low temperature solid oxide fuel cell. Materials Today Energy. **16**, 100418, **2020**.
9. RAZA M.W., KIRAN S., RAZAQ A., IQBAL M.F., HASSAN A., HUSSAIN S., ASHIQ M.N., MENG Z. Strategy to enhance the electrochemical characteristics of lanthanum sulfide nanorods for supercapacitor applications. Journal of Nanoparticle Research. **23**, 1, **2021**.
10. TAHIRA M., BATOOL F., NOREEN S., MUSTAQEEM M., MUNAWAR K.S., KANWAL S., SHAHBAZ K., ARSHAD A., ALI H.M. Unlocking the potential of de-oiled seeds of Citrus sinensis loaded with metal nanoparticles for Congo red degradation and removal: a green water treatment strategy with bibliometric analysis. Frontiers in Sustainable Food Systems. **8**, 1430624, **2024**.
11. ULLAH H., ALOMAR T.S., HUSSAIN S., SHEHZAD F.K., MUNAWAR K.S., ALMASOUD N., AMMAR M., ASIF H.M., SOHAIL M., AJMAL M. Polyoxometalate based ionic liquids reinforced on magnetic nanoparticles: A sustainable solution for microplastics and heavy metal ions elimination from water. Microchemical Journal. **204**, **2024**.
12. SENTHILKUMAR V., NISHA S., SARAVANAN M. A Review on Strontium Oxide Nanoparticles. World News of Natural Sciences. **50** 147, **2023**.
13. KOŁODZIEJSKA B., STĘPIEŃ N., KOLMAS J. The influence of strontium on bone tissue metabolism and its application in osteoporosis treatment. International Journal of Molecular Sciences. **22** (12), 6564, **2021**.
14. MUKHERJEE S., MISHRA M. Application of strontium-based nanoparticles in medicine and environmental sciences. Nanotechnology for Environmental Engineering. **6** (2), 1, **2021**.
15. RAFIQUE S., HUSSAIN S., AHMAD M., AMJAD M. Syntheses, characterization and applications of silver nanoparticles. Journal of Chemical Research Advances. **2** (2), 20, **2021**.
16. PALANISAMY M., KALIYANNAN G.V., KUMAR

H.M. Inorganic materials and their processing techniques. In: Materials for Solar Energy Conversion: Materials, Methods and Applications, chapter 8, p. 189, **2021**.
17. YING S., GUAN Z., OFOEGBU P.C., CLUBB P., RICO C., HE F., HONG J. Green synthesis of nanoparticles: Current developments and limitations. Environmental Technology & Innovation. **26**, 102336, **2022**.
18. HUSSAIN S., ALI MUAZZAM M., AHMED M., AHMAD M., MUSTAFA Z., MURTAZA S., ALI J., IBRAR M., SHAHID M., IMRAN M. Green synthesis of nickel oxide nanoparticles using Acacia nilotica leaf extracts and investigation of their electrochemical and biological properties. Journal of Taibah University for Science. **17** (1), 2170162, **2023**.
19. YASMEEN G., HUSSAIN S., TAJAMMAL A., MUSTAFA Z., SAGIR M., SHAHID M., IBRAR M., ELQAHTANI Z.M., IQBAL M. Green Synthesis of Cr_2O_3 Nanoparticles by Cassia Fistula, their Electrochemical and Antibacterial Potential. Arabian Journal of Chemistry. **16**, 104912, **2023**.
20. ANBU P., GOPINATH S.C., SALIMI M.N., LETCHUMANAN I., SUBRAMANIAM S. Green synthesized strontium oxide nanoparticles by Elodea canadensis extract and their antibacterial activity. Journal of Nanostructure in Chemistry. **12** (3), **2021**.
21. APSANA G., GEORGE P., DEVANNA N., YUVASRAVANA R. Biomimetic synthesis and antibacterial properties of strontium oxide nanoparticles using Ocimum sanctum leaf extract. Asian Journal of Pharmaceutical and Clinical Research. **11**, 384, **2018**.
22. SHIMI A.K., PARVATHIRAJ C., KUMARI S., DALAL J., KUMAR V., WABAIDUR S.M., ALOTHMAN Z.A. Green synthesis of SrO nanoparticles using leaf extract of Albizia julibrissin and its recyclable photocatalytic activity: an eco-friendly approach for treatment of industrial wastewater. Environmental Science: Advances. **1** (5), 849, **2022**.
23. GUNGOR A.A., NADAROGLU H., GULTEKIN D.D. Synthesis and characterization of nano-strontium oxide (SrO) Using erzincan cimin grape (Vitis vinifera, Cimin). Chemical Science International Journal. **26**, 1, **2019**.
24. HUSSAIN S., ZAHID A., IMRAN M., MASSEY S., RIAZ M., SAGIR M., SHAHID M., MNIF W., IQBAL S., IQBAL M. Unveiling the chemical profile, synergistic antibacterial and hemolytic effects of Cymbopogon citratus and Tachyspermum ammi leaves. Biocatalysis and Agricultural Biotechnology. **58**, 103221, **2024**.
25. SARMIN S., ETHIRAJ B., TAREK M., RENGARAJU B., KARIM K., ONG H., ABDULLAH H., KHAN M. Palm oil derived alkyd resin synthesis catalyzed by SrO/Sr (OH) 2 nanoparticles. Journal of Critical Reviews. **7** (6), **2020**.
26. AHMAD F., BELKHEDKAR M., SALODKAR R. Physical properties of nanostructured strontium oxide thin film grown by chemical bath deposition technique. AIP Publishing. **2018**.
27. LIU F., REN J., ZHAO W., LI G., JIA J. Tribological properties of NiMo matrix composite containing in-situ formed Sr2NiMoO6 and SrO at elevated temperatures. Journal of Materials Research and Technology. **22**, 2600, **2023**.
28. HUMBE A.V., UNDRE P.G., KOUNSALYE J.S., RASKAR N.D., MANE V.A., DOLE B.N. Deciphering the characterization of Ni0. 7− x Zn0. 3Mg x Fe2O4 nano ferrites: spectroscopic evaluation of structural parameters via Debye-Scherrer, Williamson-Hall, size-strain, Halder-Wagner plot, and optical methods. Journal of Materials Science: Materials in Electronics. **35** (23), 1589, **2024**.
29. JOUDEH N., LINKE D. Nanoparticle classification, physicochemical properties, characterization, and applications: a comprehensive review for biologists. Journal of Nanobiotechnology. **20** (1), 262, **2022**.
30. ABD-ELHAMID A., ABU ELGOUD E., ALY H. Sorption behavior of strontium ions by graphene oxide decorated with chitosan nanoparticles from aqueous solutions. Cellulose. **31** (13), 8203, **2024**.
31. SABOURI Z., FEREYDOUNI N., AKBARI A., HOSSEINI H.A., HASHEMZADEH A., AMIRI M.S., KAZEMI OSKUEE R., DARROUDI M. Plant-based synthesis of NiO nanoparticles using salvia macrosiphon Boiss extract and examination of their water treatment. Rare Metals. **39**, 1134, **2020**.
32. FAN D., YIN M., WANG K., WANG Z., LI H., HU H., GUO F., FENG Z., LI J., ZHANG D. The transition from indirect band gap to direct band gap and effectively separating of electron-hole pairs in h-BC2N/MoSi2N4 heterojunction for photocatalytic water splitting. International Journal of Hydrogen Energy. **2024**.
33. ARIF M., YASIN G., SHAKEEL M., MUSHTAQ M.A., YE W., FANG X., JI S., YAN D. Highly active sites of NiVB nanoparticles dispersed onto graphene nanosheets towards efficient and pH-universal overall water splitting. Journal of Energy Chemistry. **58**, 237, **2021**.